Ecotoxicology and Environmental Safety 173 (2019) 401–410

Contents lists available at ScienceDirect

Ecotoxicology and Environmental Safety

journal homepage: www.elsevier.com/locate/ecoenv

Dosimetric evaluation of individuals to ^{238}U series, ^{232}Th series and ^{40}K radionuclides present in Brazilian ornamental rocks using computational simulation

Marco A.M. Pereira[a], Lucas M. Silveira[a], Felix Nannini[a], Lucio P. Neves[b,c], Ana P. Perini[b,c], Carla J. Santos[c], Walmir Belinato[e], William S. Santos[b,d,*]

[a] Instituto de Geografia, Universidade Federal de Uberlândia, Monte Carmelo, MG, Brazil
[b] Instituto de Física, Universidade Federal de Uberlândia, Uberlândia, MG, Brazil
[c] Programa de Pós-Graduação em Engenharia Biomédica, Faculdade de Engenharia Elétrica, Universidade Federal de Uberlândia, Uberlândia, MG, Brazil
[d] Instituto de Pesquisas Energéticas e Nucleares, Comissão Nacional de Energia Nuclear (IPEN-CNEN/SP), São Paulo, SP, Brazil
[e] Instituto Federal da Bahia (IFBA), Departamento de ensino, Vitória da Conquista, BA, Brazil

ARTICLE INFO

Keywords:
Ornamental rock
Natural radioactivity
Dosimetry
Monte Carlo simulation
Virtual anthropomorphic phantoms

ABSTRACT

Granites are widely used in construction and they may be potential sources of ionizing radiation, due to the presence of radionuclides such as ^{40}K and decay products from ^{238}U series and ^{232}Th series. These radionuclides occur in the minerals constituting the rocks. To evaluate the doses in humans exposed to ^{40}K, and decay products from ^{238}U series and ^{232}Th series γ radiation, a room with dimensions of $4.0 \times 5.0 \times 2.8\ m^3$, with uniformly distributed radiation source on the floor of granitic rocks, was computationally modeled. Adult individuals were represented in the virtual scenario by two virtual anthropomorphic phantoms FASH3 and MASH3, incorporated simultaneously in the software MCNPX 2.7.0. The mean energy deposited on each organ and tissue of FASH3 and MASH3 phantoms was determined using the MCNPX *F6* tally (MeV/g/particle), while the photon flux within the room was calculated with the MCNPX *F4* tally (MeV/cm^2/particle). The organs that obtained the highest conversion coefficients CC[H_T] (Sv/Gy) were the red bone marrow (0.94), skin (0.90), breast (0.81) and bladder (0.73) for the FASH3; skin (0.89), gonads (0.88), breast (0.79) and bladder (0.70) for the MASH3. The simulated air absorbed dose rates varied between 23.4 (11%) and 25.8 (12%) nGy/h, and the annual dose rates were 0.10 (6%) and 0.11 (6%) mSv/year. These results presented acceptable statistical uncertainties and they are in agreement with the literature. Fluency of photons pointed to the central region of the room floor as the place of greatest exposure. The results showed that the organs closer to the radiation source had the highest deposited energy values. Based on the annual effective dose data obtained, it was possible to note that the values are within the literature. We believe that the methodology used will allow the investigation of any ornamental material that emits natural radiation.

1. Introduction

The production of ornamental rocks in Brazil is world-renowned. Granite rocks represent great importance in the ornamental market, being used inside domestic and commercial residences. These types of rocks have high strength, durability, mineral cohesion and they are, therefore, used as inner coating on floors and other finishes in commercial and residential constructions. Generally, these rocks contain high concentrations of natural radionuclides, mainly those from the uranium (^{238}U) and thorium (^{232}Th) radioactive decay series and the radioactive isotope of potassium (^{40}K), which are sources of population exposure to ionizing radiation. Therefore, it is necessary to quantify the doses received by individuals from their radioactive decay. It is also important to evaluate the ionizing radiation effects on humans in direct contact with natural radiation indoors (UNSCEAR, 2010; Malanca et al., 1995; Abbasi, 2013; Pavlidou et al., 2006; Xinwei et al., 2006).

In Brazil, the states of Mato Grosso, Ceará and Espírito Santo represent great importance in the scenario of national production of

* Corresponding author at: Instituto de Física, Universidade Federal de Uberlândia, Uberlândia, MG, Brazil.
E-mail addresses: marco_geologo@ufu.br (M.A.M. Pereira), lucas.morato95@ufu.br (L.M. Silveira), felixnannini@ufu.br (F. Nannini), lucio.neves@ufu.br (L.P. Neves), anapaula.perini@ufu.br (A.P. Perini), carlagracinobio@ufu.br (C.J. Santos), walmir@ifba.edu.br (W. Belinato), william@ufu.br (W.S. Santos).

https://doi.org/10.1016/j.ecoenv.2019.02.038
Received 25 September 2018; Received in revised form 9 February 2019; Accepted 12 February 2019
Available online 21 February 2019

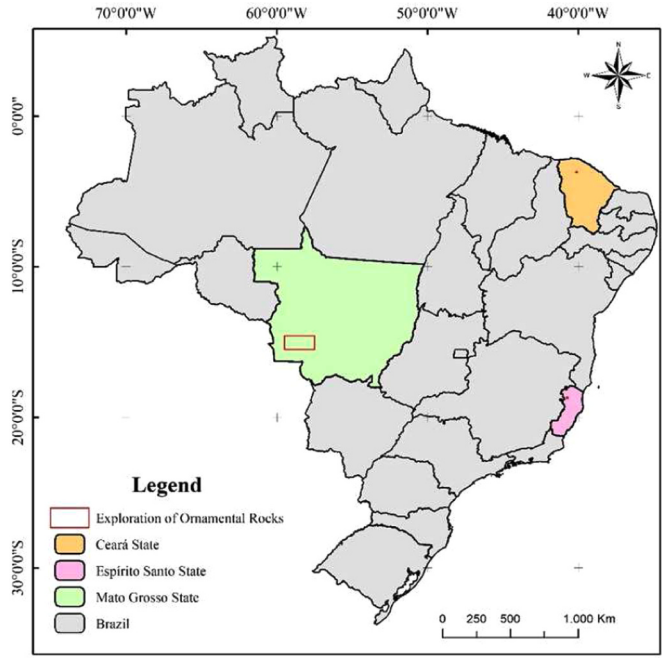

Fig. 1. State boundaries with respective areas of Brazilian ornamental rocks exploration, used in the study. Data from Cavalcante et al. (2003); Servico Geológico do Brasil (CPRM) (2007).

ornamental rocks. The rocks studied in the state of Ceará correspond to the Granítico do Barriga stock, formed by sienogranites and monzogranites (Mattos et al., 2013). The rocks from the State of Espírito Santo, originals of the Carlos Chagas Suite, are formed by Gnaisse Garnet (Saar et al., 2015). Those from the Mato Grosso state are the Monzo-Syenogranite, Anfibolite and Diabase.

The geotectonic diversity in Brazil provides the occurrence of rocks such as: marble, limestone, sandstone, quartzite, slate, gneiss and granite, widely used in civil construction. Although, the benefits of commercializing these types of rocks are enormous, it is important to know the radiation levels emitted by these granites on population exposures, since most people spend 80% of their life time indoors and, therefore, several studies are being done around the world to determine radiation doses in these individuals (Papaefthymiou and Gouseti, 2008; El-Taher, 2010; Al-Jundi et al., 2009; Baykara et al., 2011; Dziri et al., 2013).

Differently from other studies, this work, simultaneously evaluated the exposures of a woman and man adults, using Monte Carlo simulation, represented by two virtual anthropomorphic phantoms, positioned inside a closed room, with commercial granite flooring emitting gamma radiation due to ^{40}K, ^{238}U series and ^{232}Th series radionuclides. It is also import to note that when the indoor living time is taken into account, the radiological exposition must be carefully evaluated, even for low dose rates. To determine these dose rates, the granitic materials, presented in the walls, floor, and other structural components must be evaluated (Jun et al., 2014).

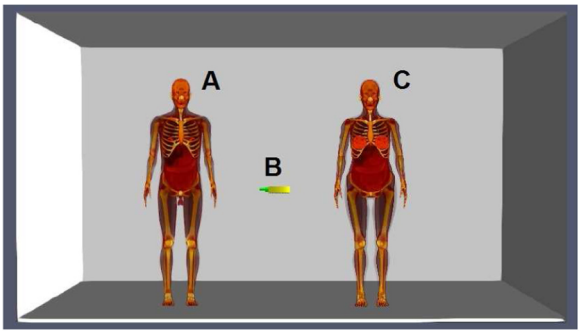

Fig. 2. Computational modeling of the exposure scenario composed by MASH3 (A), Geiger-Müller (B) and FASH3 (C) inside a living room with commercial granite floor.

Table 2
Photon energy and probability for the ^{40}K, ^{238}U series and ^{232}Th series radionuclides. Data obtained from Mustonen (1984).

^{238}U series		^{232}Th series		^{40}K	
E (MeV)	Intensity	E (MeV)	Intensity	E (MeV)	Intensity
0.047	0.040	0.040	0.015	1.460	0.107
0.053	0.022	0.100	0.023		
0.186	0.040	0.129	0.034		
0.242	0.084	0.209	0.045		
0.273	0.059	0.239	0.450		
0.295	0.207	0.270	0.032		
0.352	0.348	0.289	0.057		
0.395	0.012	0.331	0.190		
0.470	0.021	0.409	0.019		
0.609	0.430	0.463	0.046		
0.666	0.029	0.511	0.086		
0.773	0.077	0.583	0.300		
0.806	0.021	0.727	0.072		
0.934	0.036	0.782	0.091		
1.120	0.159	0.860	0.051		
1.246	0.083	0.911	0.260		
1.390	0.092	0.969	0.172		
1.509	0.037	1.588	0.066		
1.661	0.020	1.626	0.041		
1.760	0.180	2.615	0.352		
1.848	0.027				
2.118	0.011				
2.204	0.062				
2.435	0.024				

Table 1
Petrographic classification and physical property of the Brazilian ornamental rocks considered in this study (Mattos et al., 2013, Saar et al., 2015; Silva et al., 2009).

Sample Code	Brazilian State	Petrographic classification	Commercial name	Density (g cm^{-3})
OR-01	Ceará	Syenite	Rosa Iracema	2.619
OR-02	Ceará	Monzogranite	Rosa Olinda	2.632
OR-03	Ceará	Syenogranite	Branco Savana	2.614
OR-04	Ceará	Syenogranite	Branco Cristal Quartzo	2.616
OR-05	Espírito Santo	Syenogranite	Giallo São Francisco	2.636
OR-06	Espírito Santo	Gnaiss	Branco Dallas	2.632
OR-07	Espírito Santo	Gnaiss	Branco Marfim	2.631
OR-08	Mato Grosso	Monzo-syenogranite	Granito Sararé	2.590
OR-09	Mato Grosso	Anfibolite	Anfibolito Canaã	3.120
OR-10	Mato Grosso	Diabase	Diabásio Salto do Céu	2.850
Average				2.694
Min-Max				2.590–3.120

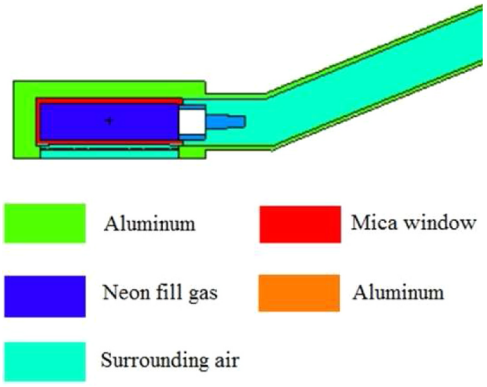

Fig. 3. Two-dimensional rendering of the pancake probe head simulated in this work.

2. Materials and methods

2.1. Characterization of the samples and region

Fig. 1 shows the location and geological insertion of the Brazilian rocks, used in this study. We evaluated four ornamental rocks, from the state of Ceará, three ornamental rocks from the state of Espírito Santo and three ornamental rocks from the state of Mato Grosso, all of granitic composition.

2.2. Computational exposition scenarios

In this study, we used a FASH3 (female) and MASH3 (male) virtual anthropomorphic phantoms to represent the exposure of individuals to γ radiation. They were also employed to determine the dose distribution inside a concrete wall room, with dimensions of (4.0 × 5.0 × 2.8) m^3, which has a rock floor of granitic composition containing ^{40}K, ^{238}U series and ^{232}Th series radionuclides. These phantoms have a detailed description of the human anatomy, including organs, and other structures, formed with 0.24 cm edges each. The FASH3 has body mass and height of 60 kg and 162.5 cm, respectively, while MASH3 has 72.7 kg and 175.6 cm. More information about these phantoms can be found elsewhere (Cassola et al., 2010a, 2010b).

To model the computational scenarios, a analysis of the three regions was undertaken. Ten different types of rocks were considered in this study, and they are all listed in Table 1. Commercial granite stones have generally 3.0 cm thick and (30 × 50) cm^2 in dimensions. The virtual phantoms were coupled to the radiation transport code MCNPX 2.7.0 (Pelowitz, 2011), which simulates the interaction of photons with the walls, air inside the room and all materials of the organs and tissues of the virtual anthropomorphic phantoms. Fig. 2 shows the model of computational exposure with the two of phantoms, representing a man and woman, inside a room with a 3 cm thick granitic floor. This floor was considered as a uniformly distributed radioactive source which emits photons in all directions. The photons emitted from ^{40}K, ^{238}U series and ^{232}Th series radionuclides are listed in Table 2.

The mean energy deposited on each organ and tissue of the FASH3 and MASH3 phantoms was determined using the MCNPX *F6* tally (MeV/ g/particle), while the photon fluence, inside the room, was calculated with the MCNPX *F4* tally (MeV/cm^2/particle) using the DE/DF response function card. The dosimetric evaluation presented by this study was based on conversion coefficients (CC) for equivalent (CC[H_T]) and effective (CC[E]) doses, normalized by the air kerma (K_{air}). The K_{air} was simulated by a Geiger-Müller (GM) counter positioned between the two anthropomorphic phantoms and located 1 m from the room's floor. The details of the materials used in GM modeling are shown in Fig. 3.

The CC[E], which is the main quantity of radiation protection, was calculated using Eq. (1).

$$CC[E] = \frac{E}{K_{air}} = \sum_T w_T \frac{CC[H_T^{MASH3}] + CC[H_T^{FASH3}]}{2} \quad (1)$$

where w_T is the tissue weighting factor and $CC[H_T^{MASH3}]$ and $CC[H_T^{FASH3}]$ are the conversion coefficients for equivalent dose of man and woman, respectively.

Using the mean value of the CC[E], which was calculated based on the equivalent dose values for organs and tissues, we estimated the mean annual dose rate, and compared it with the methodology presented by UNSCEAR (2010), which is described in Eq. (2).

$$E(mSv/year) = D(nGy/h) \times 8766(h/year) \times 0.7(Sv/Gy) \times 0.8 \times 10^{-6} \quad (2)$$

where $D(nGy/h)$ is the absorbed dose rate in the air inside the room,

Table 3
CC[H_T] and CC[E] for the MASH3 and FASH3 phantoms, due to the OR-1 Brazilian ornamental rock. Remainder Tissues are: Adrenal glands, extra thoracic region (farynx + larynx), gall bladder wall, kidneys, lymph nodes, muscle, oral cavity, pancreas, small intestine wall, spleen, thymus, uterus (female) and heart. Uncertainties are presented in parenthesis (in %).

Organs	MASH3			FASH3		
	^{40}K Sv/Gy	^{238}U series Sv/Gy	^{232}Th series Sv/Gy	^{40}K Sv/Gy	^{238}U series Sv/Gy	^{232}Th series Sv/Gy
Bone marrow	6.6E−01 (1)	6.6E−01 (1)	6.7E−01 (1)	9.4E−01 (1)	9.0E−01 (1)	9.3E−01 (1)
Colon	6.7E−01 (1)	6.4E−01 (1)	6.6E−01 (1)	6.6E−01 (1)	6.4E−01 (1)	6.5E−01 (1)
Lung	6.5E−01 (1)	6.2E−01 (1)	6.3E−01 (1)	7.0E−01 (1)	6.7E−01 (1)	6.9E−01 (1)
Stomach Wall	6.2E−01 (1)	5.9E−01 (1)	6.1E−01 (1)	6.3E−01 (1)	6.1E−01 (1)	6.3E−01 (1)
Breast	7.9E−01 (1)	7.8E−01 (1)	7.9E−01 (2)	8.1E−01 (1)	7.9E−01 (1)	8.0E−01 (1)
Remainder tissues	5.8E−02 (1)	5.7E−02 (1)	5.8E−02 (1)	5.1E−02 (1)	4.9E−02 (1)	5.0E−02 (1)
Gonads	8.8E−01 (1)	8.5E−01 (1)	8.6E−01 (1)	6.9E−01 (1)	6.7E−01 (2)	6.7E−01 (2)
Bladder	7.0E−01 (1)	6.7E−01 (1)	6.9E−01 (1)	7.3E−01 (1)	7.0E−01 (1)	7.2E−01 (1)
Oesophagus	5.7E−01 (1)	5.4E−01 (1)	5.6E−01 (1)	6.2E−01 (1)	5.8E−01 (1)	6.0E−01 (1)
Liver	6.3E−01 (1)	6.0E−01 (1)	6.1E−01 (1)	6.4E−01 (1)	6.1E−01 (1)	6.3E−01 (1)
Thyroid	5.5E−01 (1)	5.1E−01 (2)	5.3E−01 (2)	6.4E−01 (1)	6.0E−01 (2)	6.2E−01 (2)
Bone surface	1.6E−01 (1)	1.6E−01 (1)	1.6E−01 (1)	1.3E−01 (1)	1.3E−01 (1)	1.3E−01 (1)
Brain	6.3E−01 (1)	5.9E−01 (1)	6.1E−01 (1)	6.7E−01 (1)	6.4E−01 (1)	6.5E−01 (1)
Salivary glands	2.3E−01 (1)	2.2E−01 (1)	2.3E−01 (1)	2.5E−01 (1)	2.4E−01 (1)	2.4E−01 (1)
Skin	8.9E−01 (1)	8.7E−01 (1)	8.8E−01 (1)	9.0E−01 (1)	8.8E−01 (1)	8.9E−01 (1)
Eye lens	1.8E−01 (3)	1.7E−01 (4)	1.7E−01 (4)	1.8E−01 (4)	1.7E−01 (5)	1.7E−01 (5)
CC[E] (Sv/Gy)	6.0E−01 (1)	5.8E−01 (1)	5.9E−01 (1)	6.3E−01 (2)	6.1E−01 (2)	6.2E−01 (2)

Table 4
CC[H_T] and CC[E] for the MASH3 and FASH3 phantoms, due to the OR-2 Brazilian ornamental rock. Remainder Tissues are: Adrenal glands, extra thoracic region (farynx + larynx), gall bladder wall, kidneys, lymph nodes, muscle, oral cavity, pancreas, small intestine wall, spleen, thymus, uterus (female) and heart. Uncertainties are presented in parenthesis (in %).

Organs	MASH3			FASH3		
	^{40}K Sv/Gy	^{238}U series Sv/Gy	^{232}Th series Sv/Gy	^{40}K Sv/Gy	^{238}U series Sv/Gy	^{232}Th series Sv/Gy
Bone marrow	6.6E−01 (1)	6.6E−01 (1)	6.7E−01 (1)	9.4E−01 (1)	9.0E−01 (1)	9.3E−01 (1)
Colon	6.7E−01 (1)	6.4E−01 (1)	6.6E−01 (1)	6.6E−01 (1)	6.4E−01 (1)	6.5E−01 (1)
Lung	6.5E−01 (1)	6.2E−01 (1)	6.3E−01 (1)	7.0E−01 (1)	6.7E−01 (1)	6.9E−01 (1)
Stomach wall	6.2E−01 (1)	5.9E−01 (1)	6.1E−01 (1)	6.3E−01 (1)	6.1E−01 (1)	6.3E−01 (1)
Breast	7.9E−01 (1)	7.8E−01 (1)	7.9E−01 (2)	8.1E−01 (1)	7.9E−01 (1)	8.0E−01 (1)
Remainder tissues	5.8E−02 (1)	5.7E−02 (1)	5.8E−02 (1)	5.1E−02 (1)	4.9E−02 (1)	5.0E−02 (1)
Gonads	8.8E−01 (1)	8.5E−01 (1)	8.6E−01 (1)	6.9E−01 (1)	6.7E−01 (2)	6.7E−01 (2)
Bladder	7.0E−01 (1)	6.7E−01 (1)	6.9E−01 (1)	7.3E−01 (1)	7.0E−01 (1)	7.2E−01 (1)
Oesophagus	5.7E−01 (1)	5.4E−01 (1)	5.6E−01 (1)	6.1E−01 (1)	5.8E−01 (1)	6.0E−01 (1)
Liver	6.3E−01 (1)	6.0E−01 (1)	6.1E−01 (1)	6.4E−01 (1)	6.1E−01 (1)	6.3E−01 (1)
Thyroid	5.5E−01 (1)	5.1E−01 (2)	5.3E−01 (2)	6.4E−01 (1)	6.0E−01 (2)	6.2E−01 (2)
Bone surface	1.6E−01 (1)	1.6E−01 (1)	1.6E−01 (1)	1.3E−01 (1)	1.3E−01 (1)	1.3E−01 (1)
Brain	6.3E−01 (1)	6.0E−01 (1)	6.1E−01 (1)	6.7E−01 (1)	6.4E−01 (1)	6.5E−01 (1)
Salivary glands	2.3E−01 (1)	2.2E−01 (1)	2.3E−01 (1)	2.5E−01 (1)	2.4E−01 (1)	2.4E−01 (1)
Skin	8.9E−01 (1)	8.7E−01 (1)	8.8E−01 (1)	9.0E−01 (1)	8.8E−01 (1)	8.9E−01 (1)
Eye lens	1.8E−01 (3)	1.7E−01 (4)	1.7E−01 (4)	1.8E−01 (4)	1.7E−01 (5)	1.7E−01 (5)
CC[E] (Sv/Gy)	6.0E−01 (1)	5.8E−01 (1)	5.9E−01 (1)	6.4E−01 (1)	6.1E−01 (1)	6.3E−01 (1)

Table 5
CC[H_T] and CC[E] for the MASH3 and FASH3 phantoms, due to the OR-3 Brazilian ornamental rock. Remainder Tissues are: Adrenal glands, extra thoracic region (farynx + larynx), gall bladder wall, kidneys, lymph nodes, muscle, oral cavity, pancreas, small intestine wall, spleen, thymus, uterus (female) and heart. Uncertainties are presented in parenthesis (in %).

Organs	MASH3			FASH3		
	^{40}K Sv/Gy	^{238}U series Sv/Gy	^{232}Th series Sv/Gy	^{40}K Sv/Gy	^{238}U series Sv/Gy	^{232}Th series Sv/Gy
Bone marrow	6.6E−01 (1)	6.6E−01 (1)	6.7E−01 (1)	9.4E−01 (1)	9.0E−01 (1)	9.3E−01 (1)
Colon	6.7E−01 (1)	6.4E−01 (1)	6.6E−01 (1)	6.6E−01 (1)	6.4E−01 (1)	6.5E−01 (1)
Lung	6.5E−01 (1)	6.2E−01 (1)	6.3E−01 (1)	7.0E−01 (1)	6.7E−01 (1)	6.9E−01 (1)
Stomach wall	6.2E−01 (1)	5.9E−01 (1)	6.1E−01 (1)	6.3E−01 (1)	6.1E−01 (1)	6.3E−01 (1)
Breast	7.9E−01 (1)	7.8E−01 (1)	7.9E−01 (2)	8.1E−01 (1)	7.9E−01 (1)	8.0E−01 (1)
Remainder tissues	5.8E−02 (1)	5.7E−02 (1)	5.8E−02 (1)	5.1E−02 (1)	4.9E−02 (1)	5.0E−02 (1)
Gonads	8.8E−01 (1)	8.6E−01 (1)	8.7E−01 (1)	6.8E−01 (1)	6.7E−01 (2)	6.7E−01 (2)
Bladder	7.0E−01 (1)	6.7E−01 (1)	6.9E−01 (1)	7.3E−01 (1)	7.0E−01 (1)	7.2E−01 (1)
Oesophagus	5.7E−01 (1)	5.4E−01 (1)	5.6E−01 (1)	6.2E−01 (1)	5.8E−01 (1)	6.0E−01 (1)
Liver	6.3E−01 (1)	6.0E−01 (1)	6.1E−01 (1)	6.4E−01 (1)	6.1E−01 (1)	6.3E−01 (1)
Thyroid	5.5E−01 (1)	5.1E−01 (2)	5.3E−01 (2)	6.4E−01 (1)	6.0E−01 (2)	6.2E−01 (2)
Bone surface	1.6E−01 (1)	1.6E−01 (1)	1.6E−01 (1)	1.3E−01 (1)	1.3E−01 (1)	1.3E−01 (1)
Brain	6.3E−01 (1)	5.9E−01 (1)	6.1E−01 (1)	6.7E−01 (1)	6.4E−01 (1)	6.5E−01 (1)
Salivary glands	2.3E−01 (1)	2.2E−01 (1)	2.3E−01 (1)	2.5E−01 (1)	2.4E−01 (1)	2.4E−01 (1)
Skin	8.9E−01 (1)	8.7E−01 (1)	8.8E−01 (1)	9.0E−01 (1)	8.8E−01 (1)	8.9E−01 (1)
Eye lens	1.8E−01 (3)	1.7E−01 (4)	1.7E−01 (4)	1.8E−01 (4)	1.7E−01 (5)	1.7E−01 (5)
CC[E] (Sv/Gy)	6.0E−01 (1)	5.8E−01 (1)	5.9E−01 (1)	6.3E−01 (1)	6.1E−01 (1)	6.2E−01 (1)

$0.7(Sv/Gy)$ is the conversion coefficient of absorbed to effective dose received by an adult, and 0.8 is the occupation factor for closed environments (indoor).

In this study, 1E9 particle histories were simulated to ensure an acceptable statistical uncertainties. On average, the typical CPU time of the simulations ranged from 5 to 8 h on an Intel Core i7™ processor microcomputer with 16 GB of RAM (1666 MHz).

3. Results and discussion

In this work, we determined the annual dose rates (nGy/year), as well as a set of conversion coefficients for effective (CC[E]) and equivalent (CC[H_T]) doses, normalized by the K_{air}. The CC[E] and CC[H_T] are expressed in Sv/Gy, for several organs and tissues of the adult virtual anthropomorphic phantoms. All results were determined for the radionuclides ^{40}K and from the ^{238}U and ^{232}Th decay series.

The phantoms were positioned inside a room, in direct contact with a granitic floor, containing natural isotopes of ^{40}K and from the ^{238}U series and ^{232}Th series radionuclides. We considered only the γ radiation emitted from these materials. Tally $F6$ (MeV/g/particle) was used to determine the K_{air} with the GM counter. The choice of the K_{air} as the normalizing quantity is due to its use to characterize external radiation. To the annual dose estimative of adult individuals, the UNSCEAR (2010) recommends a factor of 0.7 Sv/Gy.

The results for the CC[H_T] and CC[E] are listed in Table 3 for the OR-1 sample, Table 4 for the OR-2 sample, Table 5 for the OR-3 sample, Table 6 for the OR-4 sample, Table 7 for the OR-5 sample, Table 8 for the OR-6 sample, Table 9 for the OR-7 sample, Table 10 for the OR-8 sample, Table 11 for the OR-9 sample and Table 12 for the OR-10 sample. The highest CC[E] were for the ^{40}K. This was expected, since this radionuclide possesses the highest mean photon energy (1.461 MeV), which is also the most penetrating beam, compared to the ^{238}U series radionuclides (mean energy of 0.811 MeV) and ^{232}Th series radionuclides (mean energy of 0.883 MeV).

Table 6
CC[H_T] and CC[E] for the MASH3 and FASH3 phantoms, due to the OR-4 Brazilian ornamental rock. Remainder Tissues are: Adrenal glands, extra thoracic region (farynx + larynx), gall bladder wall, kidneys, lymph nodes, muscle, oral cavity, pancreas, small intestine wall, spleen, thymus, uterus (female) and heart. Uncertainties are presented in parenthesis (in %).

Organs	MASH3			FASH3		
	^{40}K Sv/Gy	^{238}U series Sv/Gy	^{232}Th series Sv/Gy	^{40}K Sv/Gy	^{238}U series Sv/Gy	^{232}Th series Sv/Gy
Bone marrow	6.6E−01 (1)	6.6E−01 (1)	6.7E−01 (1)	9.4E−01 (1)	9.0E−01 (1)	9.3E−01 (1)
Colon	6.7E−01 (1)	6.4E−01 (1)	6.6E−01 (1)	6.6E−01 (1)	6.4E−01 (1)	6.5E−01 (1)
Lung	6.5E−01 (1)	6.2E−01 (1)	6.3E−01 (1)	7.0E−01 (1)	6.7E−01 (1)	6.9E−01 (1)
Stomach wall	6.2E−01 (1)	5.9E−01 (1)	6.1E−01 (1)	6.3E−01 (1)	6.1E−01 (1)	6.3E−01 (1)
Breast	7.9E−01 (1)	7.8E−01 (1)	7.9E−01 (2)	8.1E−01 (1)	7.9E−01 (1)	8.0E−01 (1)
Remainder tissues	5.8E−02 (1)	5.7E−02 (1)	5.8E−02 (1)	5.1E−02 (1)	4.9E−02 (1)	5.0E−02 (1)
Gonads	8.8E−01 (1)	8.6E−01 (1)	8.7E−01 (1)	6.8E−01 (1)	6.7E−01 (2)	6.7E−01 (2)
Bladder	7.0E−01 (1)	6.7E−01 (1)	6.9E−01 (1)	7.3E−01 (1)	7.0E−01 (1)	7.2E−01 (1)
Oesophagus	5.7E−01 (1)	5.4E−01 (1)	5.6E−01 (1)	6.2E−01 (1)	5.8E−01 (1)	6.0E−01 (1)
Liver	6.3E−01 (1)	6.0E−01 (1)	6.1E−01 (1)	6.4E−01 (1)	6.1E−01 (1)	6.3E−01 (1)
Thyroid	5.5E−01 (1)	5.1E−01 (2)	5.3E−01 (2)	6.4E−01 (1)	6.0E−01 (2)	6.2E−01 (2)
Bone surface	1.6E−01 (1)	1.6E−01 (1)	1.6E−01 (1)	1.3E−01 (1)	1.3E−01 (1)	1.3E−01 (1)
Brain	6.3E−01 (1)	5.9E−01 (1)	6.1E−01 (1)	6.7E−01 (1)	6.4E−01 (1)	6.5E−01 (1)
Salivary glands	2.3E−01 (1)	2.2E−01 (1)	2.2E−01 (1)	2.5E−01 (1)	2.4E−01 (1)	2.4E−01 (1)
Skin	8.9E−01 (1)	8.7E−01 (1)	8.8E−01 (1)	9.0E−01 (1)	8.8E−01 (1)	8.9E−01 (1)
Eye lens	1.8E−01 (3)	1.7E−01 (4)	1.7E−01 (4)	1.8E−01 (4)	1.7E−01 (5)	1.7E−01 (5)
CC[E] (Sv/Gy)	6.0E−01 (1)	5.8E−01 (1)	5.9E−01 (1)	6.3E−01 (1)	6.1E−01 (1)	6.2E−01 (1)

Table 7
CC[H_T] and CC[E] for the MASH3 and FASH3 phantoms, due to the OR-5 Brazilian ornamental rock. Remainder Tissues are: Adrenal glands, extra thoracic region (farynx + larynx), gall bladder wall, kidneys, lymph nodes, muscle, oral cavity, pancreas, small intestine wall, spleen, thymus, uterus (female) and heart. Uncertainties are presented in parenthesis (in %).

Organs	MASH3			FASH3		
	^{40}K Sv/Gy	^{238}U series Sv/Gy	^{232}Th series Sv/Gy	^{40}K Sv/Gy	^{238}U series Sv/Gy	^{232}Th series Sv/Gy
Bone marrow	6.6E−01 (1)	6.6E−01 (1)	6.7E−01 (1)	9.4E−01 (1)	9.0E−01 (1)	9.3E−01 (1)
Colon	6.7E−01 (1)	6.4E−01 (1)	6.6E−01 (1)	6.6E−01 (1)	6.4E−01 (1)	6.5E−01 (1)
Lung	6.5E−01 (1)	6.2E−01 (1)	6.3E−01 (1)	7.0E−01 (1)	6.7E−01 (1)	6.9E−01 (1)
Stomach wall	6.2E−01 (1)	5.9E−01 (1)	6.1E−01 (1)	6.3E−01 (1)	6.1E−01 (1)	6.3E−01 (1)
Breast	7.9E−01 (1)	7.8E−01 (1)	7.9E−01 (2)	8.1E−01 (1)	7.9E−01 (1)	8.0E−01 (1)
Remainder tissues	5.9E−02 (1)	5.7E−02 (1)	5.8E−02 (1)	5.1E−02 (1)	4.9E−02 (1)	5.0E−02 (1)
Gonads	8.8E−01 (1)	8.5E−01 (1)	8.6E−01 (1)	6.9E−01 (1)	6.7E−01 (2)	6.7E−01 (2)
Bladder	7.0E−01 (1)	6.7E−01 (1)	6.9E−01 (1)	7.3E−01 (1)	7.0E−01 (1)	7.1E−01 (1)
Oesophagus	5.7E−01 (1)	5.4E−01 (1)	5.6E−01 (1)	6.2E−01 (1)	5.8E−01 (1)	6.0E−01 (1)
Liver	6.3E−01 (1)	6.0E−01 (1)	6.1E−01 (1)	6.4E−01 (1)	6.1E−01 (1)	6.3E−01 (1)
Thyroid	5.5E−01 (1)	5.1E−01 (2)	5.3E−01 (2)	6.4E−01 (1)	5.9E−01 (2)	6.2E−01 (2)
Bone surface	1.6E−01 (1)	1.6E−01 (1)	1.6E−01 (1)	1.3E−01 (1)	1.3E−01 (1)	1.3E−01 (1)
Brain	6.3E−01 (1)	6.0E−01 (1)	6.1E−01 (1)	6.7E−01 (1)	6.4E−01 (1)	6.5E−01 (1)
Salivary glands	2.3E−01 (1)	2.2E−01 (1)	2.3E−01 (1)	2.5E−01 (1)	2.4E−01 (1)	2.4E−01 (1)
Skin	8.9E−01 (1)	8.7E−01 (1)	8.8E−01 (1)	9.0E−01 (1)	8.9E−01 (1)	8.9E−01 (1)
Eye lens	1.8E−01 (3)	1.7E−01 (4)	1.7E−01 (4)	1.8E−01 (4)	1.7E−01 (5)	1.7E−01 (5)
CC[E] (Sv/Gy)	6.0E−01 (1)	5.8E−01 (1)	5.9E−01 (1)	6.4E−01 (1)	6.1E−01 (1)	6.2E−01 (1)

As observed from Tables 3 to 12, the organs that presented the highest CC[H_T] were the bone marrow, breast, gonads, bladder and skin. Considering both phantoms, the skin was the organ with the highest value, manly due to its size, covering the entire body. The organs located far from the source, as for example the brain, salivary glands, eye lens and thyroid, presented CC[H_T] lower than organs located near the floor, as gonads and bladder.

The CC values for the mean effective dose (Sv/Gy) were determined as the mean CC[E] value of the MASH3 and FASH3, from Tables 3 to 12, and presented in Table 13.

The mean CC[E] values, from all ten Brazilian ornamental rocks evaluated in this study (Table 13) was 0.62 (2%) Sv/Gy for the ^{40}K, 0.60 (2%) Sv/Gy for the ^{238}U series radionuclides and 0.61 (2%) Sv/Gy for the ^{232}Th series radionuclides (mean value 0.61 Sv/Gy). We compared our results with previous studies, from the literature, from Zankl et al. (1997) and Krstić and Nikezić (2010), who used mathematical male and female adult phantoms, exposed to natural radionuclides evenly distributed in soil. The CC[E] values (in Sv/Gy) from Zankl et al. (1997) are 0.71 (^{40}K), 0.67 (^{238}U series) e 0.69 (^{232}Th series) (mean value 0.69 Sv/Gy); and the values from Krstić and Nikezić (2010) were 0.50 (^{238}U series), 0.52 (^{232}Th series) and 0.46 Sv/Gy (^{40}K) (mean value 0.49 Sv/Gy). As can be seen, the results are in agreement with the ones presented in this paper.

The differences may be attributed to the differences in the phantom's geometry. Those used in this paper were developed using a mesh based methodology, while in the papers of Zankl et al. (1997) and Krstić and Nikezić (2010), mathematical based virtual anthropomorphic phantoms were employed. These phantoms have organs and structures represented by mathematical equations, which leads to limitations in the accuracy of the organs geometries, as well as the materials employed to each organ/structure (only six). Besides that, Zankl et al. (1997) and Krstić and Nikezić (2010) used w_T values obtained from ICRP 60 (1990), while we used more recent values from ICRP 103 (2007).

Table 8
CC[H_T] and CC[E] for the MASH3 and FASH3 phantoms, due to the OR-6 Brazilian ornamental rock. Remainder Tissues are: Adrenal glands, extra thoracic region (farynx + larynx), gall bladder wall, kidneys, lymph nodes, muscle, oral cavity, pancreas, small intestine wall, spleen, thymus, uterus (female) and heart. Uncertainties are presented in parenthesis (in %).

Organs	MASH3			FASH3		
	^{40}K Sv/Gy	^{238}U series Sv/Gy	^{232}Th series Sv/Gy	^{40}K Sv/Gy	^{238}U series Sv/Gy	^{232}Th series Sv/Gy
Bone marrow	6.6E−01 (1)	6.6E−01 (1)	6.7E−01 (1)	9.4E−01 (1)	9.0E−01 (1)	9.3E−01 (1)
Colon	6.7E−01 (1)	6.4E−01 (1)	6.6E−01 (1)	6.6E−01 (1)	6.4E−01 (1)	6.5E−01 (1)
Lung	6.5E−01 (1)	6.2E−01 (1)	6.3E−01 (1)	7.0E−01 (1)	6.7E−01 (1)	6.9E−01 (1)
Stomach wall	6.2E−01 (1)	5.9E−01 (1)	6.1E−01 (1)	6.3E−01 (1)	6.1E−01 (1)	6.3E−01 (1)
Breast	7.9E−01 (1)	7.8E−01 (1)	7.9E−01 (2)	8.1E−01 (1)	7.9E−01 (1)	8.0E−01 (1)
Remainder tissues	5.8E−02 (1)	5.7E−02 (1)	5.8E−02 (1)	5.1E−02 (1)	4.9E−02 (1)	5.0E−02 (1)
Gonads	8.7E−01 (1)	8.5E−01 (1)	8.6E−01 (1)	6.9E−01 (1)	6.7E−01 (2)	6.7E−01 (2)
Bladder	7.0E−01 (1)	6.7E−01 (1)	6.9E−01 (1)	7.3E−01 (1)	7.0E−01 (1)	7.2E−01 (1)
Oesophagus	5.7E−01 (1)	5.4E−01 (1)	5.6E−01 (1)	6.1E−01 (1)	5.8E−01 (1)	6.0E−01 (1)
Liver	6.3E−01 (1)	6.0E−01 (1)	6.1E−01 (1)	6.4E−01 (1)	6.1E−01 (1)	6.3E−01 (1)
Thyroid	5.5E−01 (1)	5.1E−01 (2)	5.3E−01 (2)	6.4E−01 (1)	6.0E−01 (2)	6.2E−01 (2)
Bone surface	1.6E−01 (1)	1.6E−01 (1)	1.6E−01 (1)	1.3E−01 (1)	1.3E−01 (1)	1.3E−01 (1)
Brain	6.3E−01 (1)	5.9E−01 (1)	6.1E−01 (1)	6.7E−01 (1)	6.4E−01 (1)	6.5E−01 (1)
Salivary glands	2.3E−01 (1)	2.2E−01 (1)	2.3E−01 (1)	2.5E−01 (1)	2.4E−01 (1)	2.4E−01 (1)
Skin	8.9E−01 (1)	8.7E−01 (1)	8.8E−01 (1)	9.0E−01 (1)	8.8E−01 (1)	8.9E−01 (1)
Eye lens	1.8E−01 (3)	1.7E−01 (4)	1.7E−01 (4)	1.8E−01 (4)	1.7E−01 (5)	1.7E−01 (5)
CC[E] (Sv/Gy)	6.0E−01 (1)	5.8E−01 (1)	5.9E−01 (1)	6.3E−01 (1)	6.1E−01 (1)	6.2E−01 (1)

Table 9
CC[H_T] and CC[E] for the MASH3 and FASH3 phantoms, due to the OR-7 Brazilian ornamental rock. Remainder Tissues are: Adrenal glands, extra thoracic region (farynx + larynx), gall bladder wall, kidneys, lymph nodes, muscle, oral cavity, pancreas, small intestine wall, spleen, thymus, uterus (female) and heart. Uncertainties are presented in parenthesis (in %).

Organs	MASH3			FASH3		
	^{40}K Sv/Gy	^{238}U series Sv/Gy	^{232}Th series Sv/Gy	^{40}K Sv/Gy	^{238}U series Sv/Gy	^{232}Th series Sv/Gy
Bone marrow	6.6E−01 (1)	6.6E−01 (1)	6.7E−01 (1)	9.4E−01 (1)	9.0E−01 (1)	9.3E−01 (1)
Colon	6.7E−01 (1)	6.4E−01 (1)	6.6E−01 (1)	6.6E−01 (1)	6.4E−01 (1)	6.5E−01 (1)
Lung	6.5E−01 (1)	6.2E−01 (1)	6.3E−01 (1)	7.0E−01 (1)	6.7E−01 (1)	6.9E−01 (1)
Stomach wall	6.2E−01 (1)	5.9E−01 (1)	6.1E−01 (1)	6.3E−01 (1)	6.1E−01 (1)	6.3E−01 (1)
Breast	7.9E−01 (1)	7.8E−01 (1)	7.9E−01 (2)	8.1E−01 (1)	7.9E−01 (1)	8.0E−01 (1)
Remainder tissues	5.8E−02 (1)	5.7E−02 (1)	5.8E−02 (1)	5.1E−02 (1)	4.9E−02 (1)	5.0E−02 (1)
Gonads	8.7E−01 (1)	8.6E−01 (1)	8.6E−01 (1)	6.9E−01 (1)	6.7E−01 (2)	6.7E−01 (2)
Bladder	7.0E−01 (1)	6.7E−01 (1)	6.9E−01 (1)	7.3E−01 (1)	7.0E−01 (1)	7.2E−01 (1)
Oesophagus	5.7E−01 (1)	5.4E−01 (1)	5.6E−01 (1)	6.2E−01 (1)	5.8E−01 (1)	6.0E−01 (1)
Liver	6.3E−01 (1)	6.0E−01 (1)	6.1E−01 (1)	6.4E−01 (1)	6.1E−01 (1)	6.3E−01 (1)
Thyroid	5.5E−01 (1)	5.1E−01 (2)	5.3E−01 (2)	6.4E−01 (1)	6.0E−01 (2)	6.2E−01 (2)
Bone surface	1.6E−01 (1)	1.6E−01 (1)	1.6E−01 (1)	1.3E−01 (1)	1.3E−01 (1)	1.3E−01 (1)
Brain	6.3E−01 (1)	6.0E−01 (1)	6.1E−01 (1)	6.7E−01 (1)	6.4E−01 (1)	6.5E−01 (1)
Salivary glands	2.3E−01 (1)	2.2E−01 (1)	2.3E−01 (1)	2.5E−01 (1)	2.4E−01 (1)	2.4E−01 (1)
Skin	8.9E−01 (1)	8.7E−01 (1)	8.8E−01 (1)	9.0E−01 (1)	8.8E−01 (1)	8.9E−01 (1)
Eye lens	1.8E−01 (3)	1.7E−01 (4)	1.7E−01 (4)	1.8E−01 (4)	1.7E−01 (5)	1.7E−01 (5)
CC[E] (Sv/Gy)	6.0E−01 (1)	5.8E−01 (1)	5.9E−01 (1)	6.3E−01 (1)	6.1E−01 (1)	6.3E−01 (1)

We also evaluated the absorbed dose rate (nGy/h) and the effective dose rate (mSv/year), based on the absorbed doses to the organs of the MASH3 and FASH3 phantoms, employing the UNSCEAR (2010) methodology. These values were due to all radioactive materials considered in this work (^{40}K, ^{238}U series and ^{232}Th series radionuclides), contained in the granitic floor. The effective annual dose rates were determined based on the organs and tissues, with dosimetric importance, listed on the ICRP 103 (2007), in opposition to a single point of measurement, as proposed by some studies. Table 14 presents the absorbed dose rates (in nGy/h) and annual dose rate (in mSv/year) from exposition to ^{40}K, ^{238}U series and ^{232}Th series radionuclides contained in the granitic floor.

The CC values for dD/dt and dE/dt are in the range 23.4 – 25.8 nGy/h and 9.98E-02 – 1.1E-01 mSv/year, respectively. The highest values were found for the sample OR-8 ($\rho = 2.59\ g/cm^3$) and the lowest values to the sample OR-9 ($\rho = 3.12\ g/cm^3$). These differences are related to the densities of the rocks, also pointed by other studies (UNSCEAR, 2010; Risica et al., 2001). The increase in the density of the rocks leads to an increase in the photons absorption and attenuation. As a consequence, the doses above the floor will be lower, for the rocks with the highest densities.

The results of our study (Table 14) are in a reasonable agreement (within the uncertainties) with the study of El-Thaer (2010) El-Taher (2010) and Orabi (2018), that found dD/dt values of 25 and 27.7 nGy/h, respectively, for the γ emission from the ^{40}K, ^{238}U series and ^{232}Th series radionuclides.

We also observed that the dE/dt values, determined using the UNSCEAR (2010) methodology, were superior to those calculated employing the MASH3 and FASH3 virtual anthropomorphic phantoms, in this work. This may be attributed to the high conversion factor (0.7 Sv/Gy), calculated for individuals exposed to soils contaminated by natural radionuclides. From the annual exposition limit, it is very safe. However, it does not take into account the doses to the organs, which are very important for radiological protection.

Table 10
CC[H_T] and CC[E] for the MASH3 and FASH3 phantoms, due to the OR-8 Brazilian ornamental rock. Remainder Tissues are: Adrenal glands, extra thoracic region (farynx + larynx), gall bladder wall, kidneys, lymph nodes, muscle, oral cavity, pancreas, small intestine wall, spleen, thymus, uterus (female) and heart. Uncertainties are presented in parenthesis (in %).

Organs	MASH3			FASH3		
	^{40}K Sv/Gy	^{238}U series Sv/Gy	^{232}Th series Sv/Gy	^{40}K Sv/Gy	^{238}U series Sv/Gy	^{232}Th series Sv/Gy
Bone marrow	6.6E−01 (1)	6.6E−01 (1)	6.7E−01 (1)	9.4E−01 (1)	9.0E−01 (1)	9.3E−01 (1)
Colon	6.6E−01 (1)	6.4E−01 (1)	6.6E−01 (1)	6.6E−01 (1)	6.4E−01 (1)	6.6E−01 (1)
Lung	6.5E−01 (1)	6.2E−01 (1)	6.4E−01 (1)	7.0E−01 (1)	6.7E−01 (1)	6.9E−01 (1)
Stomach wall	6.2E−01 (1)	6.0E−01 (1)	6.1E−01 (1)	6.3E−01 (1)	6.1E−01 (1)	6.3E−01 (1)
Breast	7.9E−01 (1)	7.7E−01 (1)	7.9E−01 (2)	8.0E−01 (1)	7.9E−01 (1)	8.1E−01 (1)
Remainder tissue	5.8E−02 (1)	5.7E−02 (1)	5.8E−02 (1)	5.0E−02 (1)	4.9E−02 (1)	5.0E−02 (1)
Gonads	8.7E−01 (1)	8.6E−01 (1)	8.7E−01 (1)	6.8E−01 (1)	6.7E−01 (2)	6.7E−01 (2)
Bladder	7.0E−01 (1)	6.7E−01 (1)	7.0E−01 (1)	7.2E−01 (1)	7.0E−01 (1)	7.2E−01 (1)
Oesophagus	5.7E−01 (1)	5.4E−01 (1)	5.6E−01 (1)	6.1E−01 (1)	5.8E−01 (1)	6.0E−01 (1)
Liver	6.3E−01 (1)	6.0E−01 (1)	6.1E−01 (1)	6.4E−01 (1)	6.1E−01 (1)	6.3E−01 (1)
Thyroid	5.5E−01 (1)	5.1E−01 (2)	5.3E−01 (2)	6.4E−01 (1)	6.0E−01 (2)	6.2E−01 (2)
Bone surface	1.6E−01 (1)	1.6E−01 (1)	1.6E−01 (1)	1.3E−01 (1)	1.3E−01 (1)	1.3E−01 (1)
Brain	6.3E−01 (1)	5.9E−01 (1)	6.1E−01 (1)	6.7E−01 (1)	6.4E−01 (1)	6.5E−01 (1)
Salivary glands	2.3E−01 (1)	2.2E−01 (1)	2.3E−01 (1)	2.5E−01 (1)	2.4E−01 (1)	2.4E−01 (1)
Skin	8.9E−01 (1)	8.7E−01 (1)	8.8E−01 (1)	9.0E−01 (1)	8.9E−01 (1)	8.9E−01 (1)
Eye lens	1.8E−01 (3)	1.7E−01 (4)	1.7E−01 (4)	1.8E−01 (4)	1.7E−01 (5)	1.7E−01 (5)
CC[E] (Sv/Gy)	6.0E−01 (1)	5.8E−01 (1)	6.0E−01 (1)	6.3E−01 (1)	6.1E−01 (1)	6.3E−01 (1)

Table 11
CC[H_T] and CC[E] for the MASH3 and FASH3 phantoms, due to the OR-9 Brazilian ornamental rock. Remainder Tissues are: Adrenal glands, extra thoracic region (farynx + larynx), gall bladder wall, kidneys, lymph nodes, muscle, oral cavity, pancreas, small intestine wall, spleen, thymus, uterus (female) and heart. Uncertainties are presented in parenthesis (in %).

Organs	MASH3			FASH3		
	^{40}K Sv/Gy	^{238}U series Sv/Gy	^{232}Th series Sv/Gy	^{40}K Sv/Gy	^{238}U series Sv/Gy	^{232}Th series Sv/Gy
Bone marrow	6.6E−01 (1)	6.6E−01 (1)	6.7E−01 (1)	9.3E−01 (1)	9.0E−01 (1)	9.2E−01 (1)
Colon	6.6E−01 (1)	6.4E−01 (1)	6.6E−01 (1)	6.6E−01 (1)	6.4E−01 (1)	6.5E−01 (1)
Lung	6.4E−01 (1)	6.2E−01 (1)	6.3E−01 (1)	6.9E−01 (1)	6.7E−01 (1)	6.8E−01 (1)
Stomach wall	6.1E−01 (1)	6.0E−01 (1)	6.1E−01 (1)	6.3E−01 (1)	6.1E−01 (1)	6.2E−01 (1)
Breast	7.9E−01 (1)	7.9E−01 (2)	7.9E−01 (2)	8.0E−01 (1)	8.0E−01 (1)	8.0E−01 (1)
Remainder tissues	5.8E−02 (1)	5.7E−02 (1)	5.8E−02 (1)	5.0E−02 (1)	4.9E−02 (1)	5.0E−02 (1)
Gonads	8.7E−01 (1)	8.6E−01 (1)	8.6E−01 (2)	6.8E−01 (1)	6.6E−01 (2)	6.7E−01 (2)
Bladder	6.9E−01 (1)	6.8E−01 (1)	6.9E−01 (1)	7.2E−01 (1)	7.0E−01 (1)	7.1E−01 (1)
Oesophagus	5.6E−01 (1)	5.4E−01 (1)	5.6E−01 (1)	6.1E−01 (1)	5.8E−01 (1)	6.0E−01 (1)
Liver	6.2E−01 (1)	6.0E−01 (1)	6.1E−01 (1)	6.3E−01 (1)	6.1E−01 (1)	6.3E−01 (1)
Thyroid	5.4E−01 (1)	5.1E−01 (2)	5.3E−01 (2)	6.3E−01 (1)	6.1E−01 (2)	6.1E−01 (2)
Bone surface	1.6E−01 (1)	1.6E−01 (1)	1.6E−01 (1)	1.3E−01 (1)	1.3E−01 (1)	1.3E−01 (1)
Brain	6.3E−01 (1)	6.0E−01 (1)	6.1E−01 (1)	6.7E−01 (1)	6.4E−01 (1)	6.5E−01 (1)
Salivary glands	2.3E−01 (1)	2.2E−01 (1)	2.3E−01 (1)	2.5E−01 (1)	2.4E−01 (1)	2.4E−01 (1)
Skin	8.8E−01 (1)	8.8E−01 (1)	8.8E−01 (1)	8.9E−01 (1)	8.9E−01 (1)	8.9E−01 (1)
Eye lens	1.8E−01 (3)	1.7E−01 (4)	1.7E−01 (4)	1.8E−01 (4)	1.7E−01 (5)	1.8E−01 (5)
CC[E] (Sv/Gy)	6.0E−01 (1)	5.8E−01 (1)	5.9E−01 (1)	6.3E−01 (1)	6.1E−01 (1)	6.2E−01 (1)

As can be seen, from Tables 3 – 12, the CC[H_T] values present a tendency to be similar to the MASH3 and FASH3 phantoms. In addition to the genders, CC values for an organ depend on the distribution of organs in the body. The skin, which is distributed throughout the body, has the highest value in relation to the other organs and tissues evaluated. Another contributing factor is the location of the organ in relation to the radioactive source.

This is especially important for the gonads of the MASH3, which are located more in the outer part of the body and, therefore, presented a CC[H_T] higher than the female gonads, which are more in the inner part, and which have a natural shielding of other organs and structures.

After the determination of the CC[H_T], for all critical organs, the CC[E] were determined, as described in ICRP 116 (2010). The mean CC[E] calculated with MASH3 and FASH3 was 0.61 Sv/Gy, which agrees with the published result in the literature (Krstić and Nikezić, 2009).

The absorbed dose rate calculated with the GM counter was 23 nGy/h, which is close to the experimental value determined by El-Taher (2010), which was 25 nGy/h. Based on this value and the mean value of the CC[E], a mean annual effective dose rate of 0.10 mSv/year was obtained. Using Eq. (2), the value determined was 0.11 mSv/year. Therefore, these values are about 10% and 0.5% of the annual effective dose limit for exposure of public and occupational individuals, respectively.

Consequently, the use of granite in the floor construction of residences of the three studied regions, Mato Grosso, Ceará and Espírito Santo, is considered safe for the inhabitants, and may be used for all types of buildings of these three states. Even with the dosimetric values below the recommended limits, some important points should be commented: the specific activities of ^{40}K, ^{238}U series and ^{232}Th series radionuclides in ornamental rocks depend mainly on the geological, geographic and geochemical characteristics of these materials, which can affect the concentration of radionuclide in the materials (UNSCEAR, 2010). In addition, the thickness and density of the

Table 12
CC[H_T] and CC[E] for the MASH3 and FASH3 phantoms, due to the OR-10 Brazilian ornamental rock. Remainder Tissues are: Adrenal glands, extra thoracic region (farynx + larynx), gall bladder wall, kidneys, lymph nodes, muscle, oral cavity, pancreas, small intestine wall, spleen, thymus, uterus (female) and heart. Uncertainties are presented in parenthesis (in %).

Organs	MASH3			FASH3		
	^{40}K Sv/Gy	^{238}U series Sv/Gy	^{232}Th series Sv/Gy	^{40}K Sv/Gy	^{238}U series Sv/Gy	^{232}Th series Sv/Gy
Bone marrow	6.6E−01 (1)	6.6E−01 (1)	6.7E−01 (1)	9.4E−01 (1)	9.1E−01 (1)	9.2E−01 (1)
Colon	6.6E−01 (1)	6.4E−01 (1)	6.6E−01 (1)	6.6E−01 (1)	6.4E−01 (1)	6.5E−01 (1)
Lung	6.4E−01 (1)	6.2E−01 (1)	6.3E−01 (1)	6.9E−01 (1)	6.7E−01 (1)	6.8E−01 (1)
Stomach wall	6.2E−01 (1)	6.0E−01 (1)	6.1E−01 (1)	6.3E−01 (1)	6.1E−01 (1)	6.3E−01 (1)
Breast	7.9E−01 (1)	7.8E−01 (1)	7.9E−01 (2)	8.0E−01 (1)	8.0E−01 (1)	8.0E−01 (1)
Remainder tissues	5.8E−02 (1)	5.7E−02 (1)	5.8E−02 (1)	5.0E−02 (1)	4.9E−02 (1)	5.0E−02 (1)
Gonads	8.7E−01 (1)	8.6E−01 (1)	8.6E−01 (1)	6.8E−01 (1)	6.7E−01 (2)	6.6E−01 (2)
Bladder	6.9E−01 (1)	6.7E−01 (1)	6.9E−01 (1)	7.2E−01 (1)	7.1E−01 (1)	7.1E−01 (1)
Oesophagus	5.6E−01 (1)	5.4E−01 (1)	5.6E−01 (1)	6.1E−01 (1)	5.8E−01 (1)	6.0E−01 (1)
Liver	6.2E−01 (1)	6.0E−01 (1)	6.1E−01 (1)	6.3E−01 (1)	6.1E−01 (1)	6.3E−01 (1)
Thyroid	5.4E−01 (1)	5.1E−01 (2)	5.3E−01 (2)	6.4E−01 (1)	6.0E−01 (2)	6.2E−01 (2)
Bone surface	1.6E−01 (1)	1.6E−01 (1)	1.6E−01 (1)	1.3E−01 (1)	1.3E−01 (1)	1.3E−01 (1)
Brain	6.3E−01 (1)	6.0E−01 (1)	6.1E−01 (1)	6.6E−01 (1)	6.4E−01 (1)	6.5E−01 (1)
Salivary glands	2.3E−01 (1)	2.2E−01 (1)	2.3E−01 (1)	2.5E−01 (1)	2.4E−01 (1)	2.5E−01 (1)
Skin	8.8E−01 (1)	8.8E−01 (1)	8.8E−01 (1)	8.9E−01 (1)	8.9E−01 (1)	8.9E−01 (1)
Eye lens	1.8E−01 (3)	1.7E−01 (4)	1.8E−01 (4)	1.8E−01 (4)	1.7E−01 (5)	1.7E−01 (5)
CC[E] (Sv/Gy)	6.0E−01 (1)	5.8E−01 (1)	5.9E−01 (1)	6.3E−01 (1)	6.1E−01 (1)	6.2E−01 (1)

Table 13
CC values for the mean effective dose (Sv/Gy), determined as the mean values for the CC[E] of the MASH3 and the FASH3 phantoms.

Sample	^{40}K		^{238}U series		^{232}Th series	
	Sv/Gy	Unc. (%)	Sv/Gy	Unc. (%)	Sv/Gy	Unc. (%)
OR-1	6.17E−01	2	5.96E−01	2	6.09E−01	2
OR-2	6.18E−01	2	5.96E−01	2	6.10E−01	2
OR-3	6.17E−01	2	5.96E−01	2	6.10E−01	2
OR-4	6.17E−01	2	5.96E−01	2	6.09E−01	2
OR-5	6.18E−01	2	5.96E−01	2	6.09E−01	2
OR-6	6.17E−01	2	5.95E−01	2	6.09E−01	2
OR-7	6.17E−01	2	5.96E−01	2	6.10E−01	2
OR-8	6.16E−01	2	5.96E−01	2	6.10E−01	2
OR-9	6.13E−01	2	5.98E−01	2	6.08E−01	2
OR-10	6.13E−01	2	5.98E−01	2	6.08E−01	2

ornamental rock, the position in the room and the time of the occupation indoors, directly influence the dosimetric values and, consequently, the radiological risk, as point out in other studies (Risica et al., 2001).

Figs. 4, 5 and 6 shows a graphical display of the photon fluency distribution, per simulated particle inside the room, for the ^{40}K, ^{238}U series and ^{232}Th series radionuclides, respectively. The calculations were undertaken using the MCNP mesh card tally. It is possible to observe that in the central region and more close to the floor, the photon fluency is the highest.

4. Conclusions

In this study, a set of conversion coefficients for equivalent and effective doses was calculated based on the absorbed dose values in the organs and tissues of the FASH3 and MASH3 anthropomorphic phantoms, and in the absorbed dose estimated with a Geiger-Müller counter, exposed to the γ radiation emitted of the ^{40}K, ^{238}U series and ^{232}Th series radionuclides, distributed on a granite floor of a living room. Based on the dose values in organs and tissues of the anthropomorphic phantoms, the annual effective dose was calculated and compared to the result calculated using the Geiger-Müller counter.

In addition to the dosimetric results, in this study, the photon fluency, in the air inside the room, was also determined. The results indicated that the central region of the room floor is the place of the highest exposure. The use of the ornamental rocks of the three studied regions, Ceará, Espírito Santo and Mato Grosso, can be used, since they do not present health risks to the inhabitants.

Besides the CC[E] and CC[H_T], we also determined the dE/dt (in mSv/year) based on the UNSCEAR methodology, and on the equivalent doses determined over the organs. In all situations, the results from

Table 14
Absorbed dose rates (in nGy/h) and annual dose rate (in mSv/year) from exposition to ^{40}K, ^{238}U series and ^{232}Th series radionuclides contained in the granitic floor. Uncertainties are shown in parenthesis (in %).

Sample	dD/dt (nGy/h)				dE/dt (mSv/year)				UNSCEAR (2010)
	^{40}K	^{238}U series	^{232}Th series	Total	^{40}K	^{238}U series	^{232}Th series	Total	
OR-1	1.21E+01 (9)	6.76E+00 (6)	6.74E+00 (6)	2.56E+01 (12)	5.24E−02 (3)	2.82E−02 (4)	2.88E−02 (4)	1.09E−01 (6)	1.26E−01 (0.1)
OR-2	1.21E+01 (9)	6.75E+00 (6)	6.72E+00 (6)	2.55E+01 (12)	5.22E−02 (3)	2.82E−02 (4)	2.87E−02 (4)	1.09E−01 (6)	1.25E−01 (0.1)
OR-3	1.21E+01 (9)	6.77E+00 (6)	6.75E+00 (6)	2.56E+01 (12)	5.24E−02 (3)	2.83E−02 (4)	2.88E−02 (4)	1.09E−01 (6)	1.26E−01 (0.1)
OR-4	1.21E+01 (9)	6.77E+00 (6)	6.75E+00 (6)	2.56E+01 (12)	5.24E−02 (3)	2.82E−02 (4)	2.88E−02 (4)	1.09E−01 (6)	1.26E−01 (0.1)
OR-5	1.21E+01 (9)	6.74E+00 (6)	6.72E+00 (6)	2.55E+01 (12)	5.22E−02 (3)	2.81E−02 (4)	2.87E−02 (4)	1.09E−01 (6)	1.25E−01 (0.1)
OR-6	1.21E+01 (9)	6.75E+00 (6)	6.73E+00 (6)	2.56E+01 (12)	5.22E−02 (3)	2.82E−02 (4)	2.87E−02 (4)	1.09E−01 (6)	1.25E−01 (0.1)
OR-7	1.21E+01 (9)	6.75E+00 (6)	6.73E+00 (6)	2.56E+01 (12)	5.22E−02 (3)	2.82E−02 (4)	2.87E−02 (4)	1.09E−01 (6)	1.25E−01 (0.1)
OR-8	1.22E+01 (9)	6.79E+00 (6)	6.76E+00 (6)	2.58E+01 (12)	5.27E−02 (3)	2.84E−02 (4)	2.89E−02 (4)	1.10E−01 (6)	1.26E−01 (0.1)
OR-9	1.12E+01 (8)	6.11E+00 (5)	6.14E+00 (6)	2.34E+01 (11)	4.81E−02 (3)	2.56E−02 (4)	2.62E−02 (4)	9.98E−02 (6)	1.15E−01 (0.1)
OR-10	1.17E+01 (8)	6.45E+00 (6)	6.48E+00 (6)	2.46E+01 (12)	5.03E−02 (3)	2.70E−02 (4)	2.76E−02 (4)	1.05E−01 (6)	1.21E−01 (0.1)

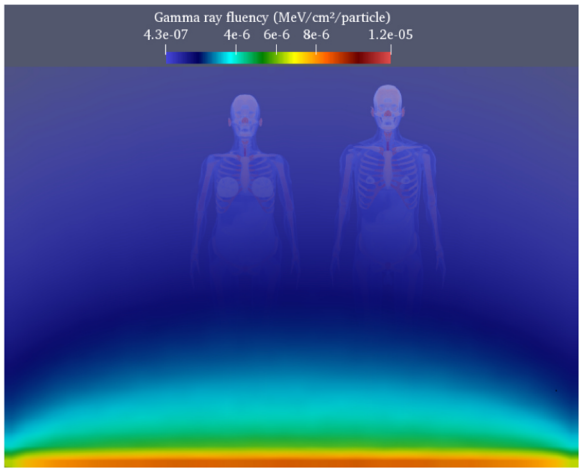

Fig. 4. Photon fluency (in MeV/cm^2/particle) simulated inside a room, with granitic rock floor with ^{40}K.

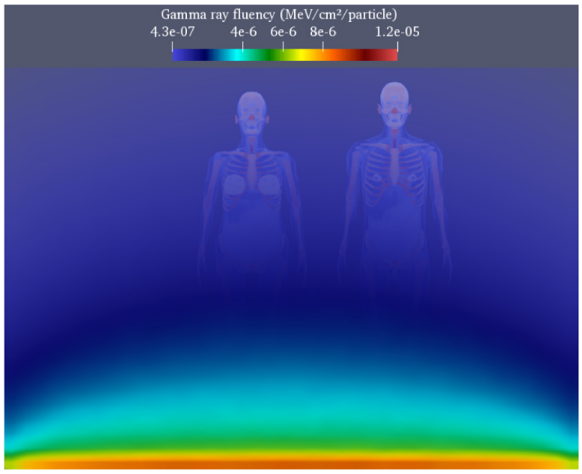

Fig. 5. Photon fluency (in MeV/cm^2/particle) simulated inside a room, with granitic rock floor with ^{238}U series radionuclides.

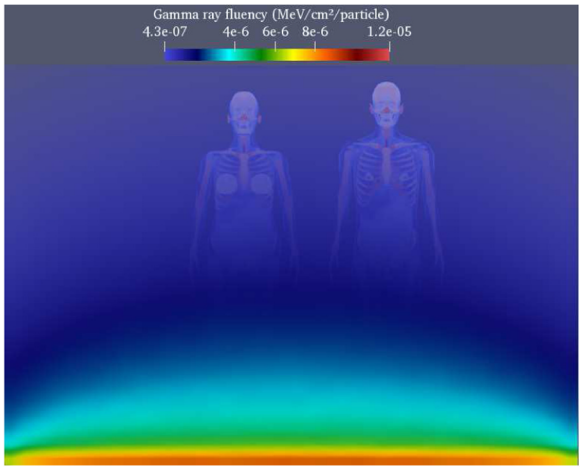

Fig. 6. Photon fluency (in MeV/cm^2/particle) simulated inside a room, with granitic rock floor with ^{232}Th series radionuclides.

UNSCEAR were higher than our values, which employed the virtual anthropomorphic phantoms. We also observed a variation in the results, as a function of the density of the granitic floor, and the type of radioactive emitter. The highest values were found for the granitic sample OR-8 ($\rho = 2.59\ g/cm^3$) and the lowest values to the granitic sample OR-9 ($\rho = 3.12\ g/cm^3$). The differences from the literature may be explained due to the differences in the methodology and types of anthropomorphic phantoms utilized.

It is hoped that the presented results may be an important tool in environmental monitoring in which people may be exposed to natural radioactivity. Besides, the new methodology, presented in this work, may be used by other studies to investigate the doses of any material used in housing construction, which emits natural radioactivity.

Acknowledgement

The authors would like to thank Dr. Richard Kramer for kindly providing the virtual anthropomorphic phantoms used in this work. This work was partially supported by the Brazilian agencies: Fundação de Amparo à Pesquisa do Estado de Minas Gerais (FAPEMIG, Grants No. APQ-03049-15 and APQ-02934-15) and Conselho Nacional de Desenvolvimento Científico e Tecnológico (CNPq Grants No. 421603/2016-0 and 420699/2016-3). William S. Santos receives a scholarship from CNPq (Grant No. 153177/2018-7).

References

Abbasi, A., 2013. Calculation of gamma radiation dose rate and radon concentration due to granites used as building materials in Iran. Radiat. Prot. Dosim. 155 (3), 335–342. https://doi.org/10.1093/rpd/nct003.

Al-Jundi, J., Ulanovsky, A., Pröhl, G., 2009. Doses of external exposure in Jordan house due to gamma-emitting natural radionuclides in building materials. J. Environ. Radioact. 100 (10), 841–846. https://doi.org/10.1016/j.jenvrad.2009.06.010.

Baykara, O., Karatepe, Ş., Doğru, M., 2011. Assessments of natural radioactivity and radiological hazards in construction materials used in Elazig, Turkey. Radiat. Meas. 46 (1), 153–158. https://doi.org/10.1016/j.radmeas.2010.08.010.

Cassola, V.F., Lima, V.J.D., Kramer, R., Khoury, H.J., 2010a. FASH and MASH: female and male adult human phantoms based on polygon mesh surfaces: I. development of the anatomy. Phys. Med. Biol. 55 (1), 133–162. https://doi.org/10.1088/0031-9155/55/1/009.

Cassola, V.F., Lima, V.J.D., Kramer, R., Khoury, H.J., 2010b. FASH and MASH: female and male adult human phantoms based on polygon mesh surfaces. part II. dosimetric calculations. Phys. Med. Biol. 55 (1), 163–189. https://doi.org/10.1088/0031-9155/55/1/010.

Cavalcante, J., Vasconcelos, A., Gomes, F., 2003. Mapa geológico do Estado do Ceará. Convênio MME/CPRM Governo do Estado do Ceará / Secretaria de Recursos Hídricos, Fortaleza (in portuguese).

Dziri, S., Nachab, A., Nourreddine, A., Sellam, A., Gelus, D., 2013. Experimental and simulated effective dose for some building materials in France. World J. Nucl. Sci. Technol. 3 (2), 41–45. https://doi.org/10.4236/wjnst.2013.32007.

El-Taher, A., 2010. Gamma spectroscopic analysis and associated radiation hazards of building materials used in Egypt. Radiat. Prot. Dosim. 138 (2), 166–173. https://doi.org/10.1093/rpd/ncp205.

ICRP 103, The 2007 Recommendations of the International Commission on Radiological Protection, Ann. 37 (2-4), 2007.

ICRP 116, 2010. Conversion Coefficients for Radiological Protection Quantities for External Radiation Exposures. 40 Ann. ICRP (2–5).

ICRP 60, 1990. 1990 Recommendations of the International Commission on Radiological Protection. 21 Ann. ICRP (1-3).

Jun, D., Lei, C., Xu, S., 2014. Monte Carlo simulation of indoor external exposure due to gamma-emitting radionuclides in building materials. Chin. Phys. C 38 (10), 108202(URL ⟨http://stacks.iop.org/1674-1137/38/i=10/a=108202⟩).

Krstić, D., Nikezić, D., 2009. External doses to humans from ^{137}Cs in soil. Health Phys. 91 (3), 249–257. https://doi.org/10.1097/01.HP.0000214136.56619.2d.

Krstić, D., Nikezić, D., 2010. Calculation of the effective dose from natural radioactivity in soil using MCNP code. Appl. Radiat. Isot. 68 (4), 946–947. https://doi.org/10.1016/j.apradiso.2009.12.018.

Malanca, A., Pessina, V., Dallara, G., Luce, C., Gaidolfi, L., 1995. Natural radioactivity in building materials from the Brazilian state of Espírito Santo. Appl. Radiat. Isot. 46 (12), 1387–1392. https://doi.org/10.1016/0969-8043(95)00223-Z.

Mattos, I., Artur, A., Neto, J.N., 2013. Caracterização petrográfica e tecnológica de granitos ornamentais do stock granítico Serra do Barriga, Sobral/CE (Petrographical and technological characterization of granites from Serra do Barriga stock, Sobral/CE). pp. 247–268 (in portuguese).

Mustonen, R., 1984. Methods for evaluation of radiation from building materials. Radiat. Prot. Dosim. 7 (1–4), 235–238. https://doi.org/10.1093/oxfordjournals.rpd.a082999.

Orabi, M., 2018. Development of a simulation model for estimating the indoor gamma radiation dose. Radiat. Phys. Chem. 147, 114–117. https://doi.org/10.1016/j.radphyschem.2018.02.016.

Papaefthymiou, H., Gouseti, O., 2008. Natural radioactivity and associated radiation hazards in building materials used in Peloponnese, Greece. Radiat. Meas. 43 (8), 1453–1457. https://doi.org/10.1016/j.radmeas.2008.03.032.

Pavlidou, S., Koroneos, A., Papastefanou, C., Christofides, G., Stoulos, S., Vavelides, M., 2006. Natural radioactivity of granites used as building materials. J. Environ. Radioact. 89 (1), 48–60. https://doi.org/10.1016/j.jenvrad.2006.03.005.

Pelowitz, D.B., 2011. MCNPX User's Manual, Version 2.7.0. Los Alamos National Laboratory (Report LA-CP-11-00438).

Risica, S., Bolzan, C., Nuccetelli, C., 2001. Radioactivity in building materials: room model analysis and experimental methods. Sci. Total Environ. 272 (1), 119–126. https://doi.org/10.1016/S0048-9697(01)00675-1. (radon in the Living Environment).

Saar, L.C.A., Godoy, A.M., Bolonini, T.M., 2015. Considerações sobre os granitos giallo São Francisco real, branco dallas e branco marfim, no município de Barra de São Francisco - ES para aplicação como rocha ornamental e de revestimento. Geociências 34 (1), 1–18 (in portuguese).

Serviço Geológico do Brasil (CPRM), 2007. Serviço Geológico do Brasil (CPRM), Geologia da Folha de Mantena - SE.24-Y-A-VI. Programa Geologia do Brasil - mapa geológico da Folha Mantena (escala 1:100.000 (in portuguese)).

Silva, J.A., Godoy, A.M., Araújo, L.M.B., 2009. Rochas ornamentais e de revestimento do sudoeste do Estado do Mato Grosso. Geociências 28 (2), 129–142.

UNSCEAR, 2010. United Nations Scientific Committee on the Effects of Atomic Radiation - Sources and Effects of Ionizing Radiation. United Nations, New York (Tech. Rep. UNSCEAR 2008).

Xinwei, L., Lingqing, W., Xiaodan, J., 2006. Radiometric analysis of Chinese commercial granites. J. Radioanal. Nucl. Chem. 267 (3), 669–673. https://doi.org/10.1007/s10967-006-0101-1.

Zankl, M., Petoussi-Henß, N., Drexler, G., Saito, K., 1997. The calculation of dose from external photon exposures using reference human phantoms and monte carlo methods – part VII: Organ doses due to parallel and environmental exposure geometries. Institut für Strahlenschutz (Tech. Rep. GSF-Bericht 8/97).